Journal of Nuclear Medicine, published on February 26, 2021 as doi:10.2967/jnumed.120.261446

Site-Specific and Residualizing Linker for ^{18}F-Labeling with Enhanced Renal Clearance: Application to an Anti-HER2 Single Domain Antibody Fragment

Zhengyuan Zhou, Rebecca Meshaw, Michael R. Zalutsky, and Ganesan Vaidyanathan*

Department of Radiology, Duke University Medical Center, Durham, North Carolina

*Corresponding Author: Ganesan Vaidyanathan, 311 Research Drive, Durham, NC 27710 Tel.: 919-684-7811; email: ganesan.v@duke.edu

First Author: Zhengyuan Zhou (Postdoctoral), 311 Research Drive, Durham, NC 27710 Tel.: 402-206-4974; email: zz89@duke.edu

Word Count: 5198

Financial Support: NIH Grants CA188177 and CA42324

Running Title: Site-specific ^{18}F-labeled sdAb

ABSTRACT

Single domain antibody fragments (sdAbs) are promising vectors for immunoPET; however, better methods for labeling sdAbs with ^{18}F are needed. Herein, we evaluate a site-specific strategy utilizing an ^{18}F residualizing motif and the anti-HER2 sdAb 5F7 bearing an engineered C-terminal GGC tail. **Methods:** 5F7GGC was site-specifically attached with a tetrazine-bearing agent via thiol-maleimide reaction. The resultant conjugate was labeled with ^{18}F by inverse electron demand Diels-Alder cycloaddition with a *trans*-cyclooctene attached to 6-^{18}F-fluoronicotinoyl moiety via a renal brush border enzyme-cleavable linker and a PEG_4 chain (^{18}F-5F7GGC). For comparisons, 5F7 sdAb was labeled using the prototypical residualizing agent, *N*-succinimidyl 3-(guanidinomethyl)-5-^{125}I-iodobenzoate (*iso*-^{125}I-SGMIB). The two labeled sdAbs were compared in paired-label studies performed in the HER2-expressing BT474M1 breast carcinoma cell line and athymic mice bearing BT474M1 subcutaneous xenografts. MicroPET/CT imaging after administration of ^{18}F-5F7GGC in the above mouse model was also carried out. **Results:** ^{18}F-5F7GGC was synthesized in an overall radiochemical yield of 8.9 ± 3.2% with retention of HER2 binding affinity and immunoreactivity. The total cell-associated and intracellular activity for ^{18}F-5F7GGC was similar to that for co-incubated *iso*-^{125}I-SGMIB-5F7. Likewise, the uptake of ^{18}F-5F7GGC in BT474M1 xenografts in mice was similar to that for *iso*-^{125}I-SGMIB-5F7; however, ^{18}F-5F7GGC exhibited significantly more rapid clearance from the kidney. MicroPET/CT imaging confirmed high uptake and retention in the tumor with very little background activity at 3 h except in the bladder. **Conclusion:** This site-specific and residualizing ^{18}F labeling strategy could facilitate clinical translation of 5F7 anti-HER2 sdAb as well as other sdAbs for immunoPET.

Key Words: single domain antibody fragment; site-specific labeling; immunoPET; click chemistry; HER2

INTRODUCTION

Smaller protein scaffolds exemplified by 6-kDa affibodies and 12-15-kDa single domain antibody fragments (sdAbs) have emerged as promising platforms for theranostics because they possess properties intermediate between those of monoclonal antibodies (mAbs) and peptides. A recent review (*1*) has summarized efforts with these delivery vehicles to image and treat cancers overexpressing epidermal growth factor receptor 2 (HER2), an internalizing receptor that is overexpressed in breast, ovarian, gastric and other cancers (*2*). Because only about 20-25% of breast cancers are HER2-positive and mestastatic disease frequently exhibits heterogeneities in HER2 expression, assessment of HER2 status is imperative before embarking on HER2-targeted therapies (*3*).

Combining an anti-HER2 sdAb with a radiolabeling strategy tuned to the properties of small proteins could provide a promising immunoPET approach for global and repeatable evaluation of HER2 status. Given the high and prolonged uptake of radiometal-labeled sdAbs in kidneys (*1,4*), ^{18}F is a promising radionuclide for sdAb-based immunoPET. Moreover, ^{18}F has a half-life compatible with the rapid clearance of sdAbs, positron emission characteristics that are ideal for imaging, and a readily available supply-chain. Although several ^{18}F protein labeling methods have been developed (*5*), *N*-succinimidyl 4-^{18}F-fluorobenzoate (^{18}F-SFB) (*6*) remains the most widely used reagent for this purpose. Both our group (*7*) and others (*8*) have labeled sdAbs with ^{18}F-SFB; however, the non-residualizing capacity of ^{18}F-SFB compromised tumor retention of ^{18}F after receptor-mediated internalization.

Studies with ^{131}I- and ^{211}At-labeled HER2-targeted sdAbs have demonstrated that very effective trapping of radioactivity in tumor can be achieved using charged prosthetic groups (*9-11*). In recent years, we have developed conceptually similar prosthetic agents for labeling sdAbs with ^{18}F (*7,12,13*). Two tactics that we investigated were the very fast tetrazine (Tz)-*trans*-

cyclooctene (TCO) inverse electron demand Diels-Alder cycloaddition reaction (IEDDAR) and exploiting a renal brush border enzyme (RBBE)-cleavable linker to reduce kidney activity (*12,14*). In these studies, ^{18}F was introduced on the Tz-bearing moiety. Although kidney activity could be reduced considerably, activity in hepatobiliary organs was elevated, presumably due to the high lipophilicity of Tz-bearing radio-catabolites (*15,16*).

Herein we describe a new linker for ^{18}F labeling of the HER2-targeted sdAb 5F7 that also could be applied in principle to site-specific labeling of other proteins with engineered cysteine residues via thiol-maleimide conjugation (*17*). Precise control of the ^{18}F labeling site on the C-terminus of an sdAb can avoid chemical modification of amino acids involved in receptor/antigen recognition and provide a uniform product more amenable to clinical translation (*18*). Other design features of this linker include the use of the 6-^{18}F-fluoronicotinoyl group for residualization (*13*), and a GlyLys RBBE-cleavable linker strategically positioned within its structure (Fig. 1) to create rapid, high contrast between tumor and both kidneys and hepatobiliary organs.

MATERIALS AND METHODS

sdAbs, Cells, Culture Conditions and Animal Model

The anti-HER2 sdAb 5F7 and 5F7GGC, its analogue with an engineered cysteine at the C-terminus (*19,20*), were purchased from ATUM.

Cell culture reagents were purchased from Thermo Fisher Scientific and InvivoGen. HER2-expressing BT474 human breast carcinoma cells and its more metastatic version, BT474M1 (*21*), were cultured in RPMI 1640 medium containing 10% FBS, 1% Penicillin-Streptomycin, 5 μg/ml plasmocin, 1% sodium pyruvate, 1% HEPES, and 0.4 μg/ml insulin.

All procedures involving animals were approved by the Duke University IACUC. Female nude mice were obtained from an internal breeding colony at Duke or from Charles River Laboratories

and subcutaneous BT474M1 xenografts were established as described (*7,11*). Biodistribution and imaging studies were initiated when tumors were 150–350 mm^3 in volume.

Synthesis, Radiosynthesis and ^{18}F-labeling of 5F7GGC

Details of the synthesis of the precursor (**7**), standard (**8**) and ^{18}F-**8** as well as the synthesis of *iso*-^{125}I-SGMIB-5F7 are provided in Supplemental Materials. First, the sdAb was reduced to convert any dimer present to monomer. For this, a slurry of immobilized tris-[2-carboxyethyl] phosphine hydrochloride gel (Thermo Fisher Scientific; 300 µl) was added to a solution of 5F7GGC (1.5 mg, 115 nmol) in 300 µl of 0.2 M NH_4OAc containing 5 mM EDTA, pH 6.3, and the mixture stirred at 37°C for 1 h. The suspension was centrifuged, and the supernatant containing monomeric 5F7GGC was immediately added to a vial containing methyltetrazine-PEG_4-maleimide (0.18 mg, 345 nmol), and the mixture stirred at 37°C for 1 h. The Tz-5F7GGC product was isolated from the mixture by size-exclusion (SE)-HPLC. For this, an Agilent PL Multisolvent 20 (7.8 mm I.D. × 150 mm) SE-HPLC column was eluted in isocratic mode with water at a flow rate of 0.9 ml/min. The pooled HPLC fractions containing the Tz-5F7GGC (t_R = 3.3 min) were lyophilized to obtain 0.5 mg of a pink solid. Its molecular weight was determined by LCMS and binding affinity to HER2-Fc by surface plasmon resonance (SPR) (Supplemental Materials). A solution of Tz-5F7GGC in PBS, pH 7.4 (50 µl, 2 mg/ml) was added to a vial containing dried ^{18}F-**8** (60–280 MBq), and the mixture incubated at 37°C for 10 min. ^{18}F-FN-PEG_4-GK-TCO-Tz-PEG_4-Mal-5F7GGC (^{18}F-5F7GGC) was isolated by gel filtration over a PD-10 column eluted with PBS (*20*). Radiochemical purity, HER2 binding affinity and immunoreactivity were determined as described previously (*12*) with details provided in Supplemental Materials.

Cellular Uptake and Internalization Assays

Paired-label uptake and internalization assays were performed on BT474M1 cells to compare the behavior of ^{18}F-5F7GGC and *iso*-^{125}I-SGMIB-5F7 sdAbs as described in Supplemental Materials.

Biodistribution Studies

The paired-label biodistribution of ^{18}F-5F7GGC and *iso*-^{125}I-SGMIB-5F7 was evaluated in athymic mice bearing subcutaneous BT474M1 xenografts. Groups of five mice received 166 kBq (0.64 µg) of *iso*-^{125}I-SGMIB-5F7 and 666 kBq (3.6 µg) of ^{18}F-5F7GGC in 100 µl PBS via the tail vein. It was necessary to use a larger amount of activity and hence the mass for ^{18}F-5F7GGC to compensate for the more rapid decay of ^{18}F. Ex vivo biodistribution was determined at 1 and 3 h, and %ID/g were calculated as described (*7*).

Micro-PET/CT Imaging

Three BT474M1 tumor-bearing mice were imaged on a Siemens Inveon PET/CT system at 1, 2 and 3 h after injection of ^{18}F-5F7GGC (1.6-2.2 MBq, 19-23 µg). Mice were anesthetized using 2–3% isoflurane in oxygen and a 5 min static PET acquisition followed by a 5 min CT scan was performed. List mode PET data were histogram-processed, and the images reconstructed using a standard OSEM3D/MAP algorithm—two OSEM3D iterations, and eighteen MAP iterations—with a cutoff (Nyquist) of 0.5. Images were corrected for attenuation (CT-based) and radioactive decay. Image analysis was performed using Inveon Research Workplace software.

Statistical Analysis

Results are reported as mean ± SD. The statistical significance of differences between co-incubated or co-administered tracers was determined by a 2-tailed, paired Student *t*-test (GraphPad QuickCalcs). A *P* value of <0.05 was considered to be significant.

RESULTS

Synthesis, sdAb Conjugation and Radiochemistry

As shown in Supplemental Fig. 1, the precursor **7** was synthesized from the known compound **1** (*22*) in six steps. Compound **8** was synthesized by treatment of **7** with TBAF in 75.4% yield. The ^{1}H-NMR and mass spectrometry data for compounds **2-8** were consistent with their

structures. Fig. 1 shows the synthesis scheme for Tz-5F7GGC and its labeling via IEDDAR with ^{18}F-**8**. SE-HPLC-MS analysis of the reaction mixture for 5F7GGC conjugation with methyltetrazine-PEG$_4$-maleimide indicated complete conversion of 5F7GGC to Tz-5F7GGC (Supplemental Fig. 2). The observed molecular weight was consistent with its structure. SPR indicated a K_d = 0.3 nM (k_a = 1.58 x 10^6 $M^{-1}s^{-1}$; k_d = 4.60 x 10^{-4} s^{-1}) for Tz-5F7GGC versus 0.2 nM for 5F7 demonstrating that attaching the Tz-PEG$_4$-Mal moiety had minimal effect on HER2 binding affinity (Fig. 2).

The radiochemical yield (RCY) for the synthesis of ^{18}F-FN-PEG$_4$-GK-TCO (^{18}F-**8**) from **7** via S_NAr reaction was 47.4 ± 9.0% (n=11). With 100 µg of protein at 2 mg/ml, the RCY for IEDDAR between Tz-5F7GGC and ^{18}F-**8** was 27.3 ± 8.2% (n=4). Although performed only twice, use of 200 µg of protein at 4 mg/ml increased conjugation yields to 46.1 ± 4.5%. Based on initial aqueous ^{18}F-fluoride activity, the total synthesis time for ^{18}F-5F7GGC was 90 min in an overall RCY of 8.9 ± 3.2% (n=6); [7.3 ± 3.3% (n=4) and 11.3 ± 0.4% (n=2) for IEDDAR with 100 µg and 200 µg sdAb, respectively]. While higher IEDDAR yields were obtained in the 200 µg syntheses, RCY for ^{18}F-**8** were low due to an HPLC malfunction. The molar activity for ^{18}F-5F7GGC was 5.2 ± 2.7 MBq/nmol (n=6). SDS-PAGE (Supplemental Fig. 3A) and SE-HPLC (Supplemental Fig. 3B) of ^{18}F-5F7GGC showed a single radioactive band/peak (~100%) corresponding to the molecular weight of an sdAb. The K_d for binding of ^{18}F-5F7GGC to BT474 cells was 3.37 ± 0.36 nM (Supplemental Fig. 3C) and its immunoreactive fraction 70.8% (Supplemental Fig. 3D), demonstrating that HER2-reactivity was not compromised with this ^{18}F labeling strategy.

Cell Uptake and Internalization Assay

After incubation with BT474M1 cells at 37°C, total cell-associated activity (Fig. 3A) for ^{18}F-5F7GGC was 24.3 ± 0.9%, 31.3 ± 0.9% and 35.3 ± 2.5% of input activity at 1, 2 and 4 h, respectively, values that were slightly lower than those for co-incubated *iso*-^{125}I-SGMIB-5F7 (25.2 ± 0.6%, 32.5 ± 0.8% and 37.1 ± 2.0%); but differences between the radio-conjugates were not

statistically significant (P>0.05). Nonspecific uptake, determined at the 2-h time point by co-incubation with excess trastuzumab, was <1% of input activity for both radiotracers. The percentage of input activity that was intracellularly trapped was 12.3 ± 0.5%, 17.3 ± 1.1% and 20.8 ± 1.5% for ^{18}F and 13.4 ± 4.4%, 18.2 ± 1.2% and 22.3 ± 1.2% for ^{125}I at 1, 2 and 4 h, respectively (Fig. 3B; P>0.05 for all).

Biodistribution

The data from the paired-label biodistribution of ^{18}F-5F7GGC and *iso*-^{125}I-SGMIB-5F7 in athymic mice bearing BT474M1 xenografts is presented in Fig. 4. Tumor uptake of ^{18}F-5F7GGC was similar to that seen for *iso*-^{125}I-SGMIB-5F7 both at 1h (^{125}I, 18.34 ± 1.62% ID/g; ^{18}F, 14.87 ± 1.41% ID/g, P<0.01) and 3 h (^{125}I, 17.20 ± 5.09% ID/g; ^{18}F, 12.92 ± 3.73% ID/g, P>0.05). On the other hand, with a few exceptions, normal tissue activity for ^{18}F-5F7GGC was similar or less than observed for *iso*-^{125}I-SGMIB-5F7. Remarkably, ^{18}F-activity levels in kidneys were 4- and 6-fold lower than those for ^{125}I at 1 and 3 h, respectively. Bone uptake of ^{18}F was low suggesting limited susceptibility of ^{18}F-5F7GGC to defluorination in vivo. Tumor-to-normal-tissue ratios for the two radiolabeled sdAbs are shown in Fig. 5. Tumor-to-kidney ratios for ^{18}F (1.2 ± 0.4 and 12.2 ± 3.5) were 3.3- and 4.5-fold higher (P<0.004) than those for ^{125}I (0.37 ± 0.05 and 2.7 ± 0.7) at 1 and 3 h, respectively. Likewise, tumor-to-blood ratios were 2-3-fold higher for ^{18}F. The tumor-to-liver ratio for ^{18}F-5F7GGC was >5:1 at 1 h and lower than that for *iso*-^{125}I-SGMIB-5F7 (P < 0.0003).

MicroPET/CT Imaging

Small-animal PET/CT MIP images of a representative mouse bearing a subcutaneous BT474M1 xenograft obtained 1, 2 and 3 h after administration of ^{18}F-5F7GGC are shown in Fig. 6. Consistent with the results from the necropsy study, pronounced tumor accumulation was observed at all time points with minimal background activity except in kidneys and bladder. Kidney activity at 1 h was quite low, nearly undetectable by 2 h and eliminated by 3 h, with bladder

having prominent activity at all time points. The average tumor uptake values (n=3) calculated from the PET imaging data, expressed as SUV_{max} (%ID/g_{max}), were 4.6 ± 0.5 (18.0 ± 1.8), 4.7 ± 0.9 (17.9 ± 3.6), and 5.0 ± 0.8 (19.0 ± 3.1) at 1, 2 and 3 h, respectively, with corresponding values for kidneys of 2.9 ± 0.3 (11.2 ± 1.0), 1.0 ± 0.1 (4.3 ± 0.6), and 0.6 ± 0.1 (2.4 ± 0.2). Tumor-to-kidney ratios calculated from these PET imaging data were 1.6 ± 0.2, 4.2 ± 0.6, and 7.8 ± 0.8 at 1, 2 and 3 h, respectively.

DISCUSSION

Small protein platforms — exemplified herein by an sdAb — have favorable properties for immunoPET including rapid tumor penetration and fast normal tissue clearance and are ideally suited for use with ^{18}F. However, because of their small size, they are much more likely than whole mAbs to be adversely affected by chemical modification, resulting in unwanted normal tissue retention and/or altered binding to their molecular target. Moreover, unlike mAbs, retention of activity in the kidneys also can be problematic. To address these issues, we designed a labeling strategy (Fig. 1) comprised of several synergistic components: a site-specific linker to control labeling location and stoichiometry (*19*), an RBBE-cleavable sequence to reduce kidney activity (*12,14*), a 6-fluoronicotinoyl group (*13,14*) to provide short-term residualization, and positioning the RBBE-cleavable sequence to avoid Tz- or TCO-bearing ^{18}F-labeled catabolites in vivo.

Site-specific conjugation of the Tz-bearing maleimide with 5F7GGC was achieved without impairing HER2 binding of the sdAb (Fig. 2). The 48% RCY for TCO-bearing ^{18}F-**8** synthesis was reasonable given the presence of the free carboxyl group active hydrogens in compound **7**, which is not generally conducive for labeling using nucleophilic ^{18}F-fluoride (*23*). Of note, ^{18}F-labeling of TCO-bearing molecules was typically performed via the S_N2 reaction whereas in our case, it was performed via the S_NAr reaction, a first. RCY for IEDDAR between Tz-5F7GGC and ^{18}F-**8**

appeared to increase with increasing protein concentration but were lower than reported for ^{18}F-labeling using Tz-TCO IEDDAR in general (*24*), and for IEDDAR between TCO-modified sdAbs and ^{18}F-labeled Tz derivatives, in particular (*12,14*). A likely factor contributing to this is the number of prosthetic moieties per sdAb available for IEDDAR — when random conjugation was employed, more than one TCO was attached per sdAb (*12,14*) versus just one Tz moiety in the current work. However, even with site-specific labeling, higher yields (53-77%) have been reported for IEDDAR between ^{18}F-TCO and a diabody site-specifically modified with a Tz moiety (*25*). Differences in solvent, protein concentration and polarity of the reagents between the two studies are noted, and these variables will be evaluated in future optimization of the current labeling strategy.

With the current procedure, the overall decay-corrected RCYs for the synthesis of ^{18}F-5F7GGC were 7.3 ± 3.3% and 11.3 ± 0.4% at 100 and 200 μg of Tz-5F7GGC, respectively, providing 154 and 237 MBq of ^{18}F-5F7GGC from 3.7 GBq of aqueous ^{18}F-fluoride in 90 min. Based on literature precedents (*24*), higher yields should be readily attainable by increasing protein levels beyond 200 μg, which should be compatible with patient use given that a 1 mg sdAb dose was used in a Phase 1 trial with another anti-HER2 sdAb labeled with ^{68}Ga (*26*). That study used an average administered activity of 107 MBq ^{68}Ga suggesting that with our current radiochemistry procedures, clinical studies would be feasible.

Multiple methods for labeling proteins with ^{18}F have been reported (*5*). Random labeling of constituent protein lysine residues can be accomplished using active esters such as *N*-succinimidyl 4-^{18}F-fluorobenzoate, 2,3,5,6-tetrafluorophenyl 6-^{18}F-fluoronicotinate (*13,27*) and their 4-nitrophenyl analogues (*28*) among others. The site-specific ^{18}F-labeling of proteins also has been described including via oxime formation with an engineered aminoxy function on the protein with 4-^{18}F-fluorobenzaldehyde or preconjugating the protein with maleimide-bearing agents containing moieties such as 4-fluorobenzaldehyde O-alkyl oxime, 4-SiFA and AlF-chelate

complex and subsequent ^{18}F-labeling of the conjugate (*29,30*). Of direct relevance to the current study, the last three approaches were evaluated for ^{18}F-labeling of an anti-HER2 affibody. Although uptake in HER2-positive xenografts was reported, there were significant problems with each ^{18}F-affibody conjugate – either high uptake in the intestines or the kidneys, or excessive in vivo defluorination. From a radiochemistry perspective, it is important to note that the maleimide functionality is susceptible to S_NAr and S_N2 ^{18}F-labeling conditions and thus the maleimide-bearing part has to be conjugated to an ^{18}F-bearing moiety, the synthesis of which often involves one or more steps. As mentioned above, an alternative approach of labeling proteins with ^{18}F using maleimide agents involves their conjugation first with the maleimide-bearing agent and then to perform the labeling under acidic pH and high temperatures (*29*); however, unfortunately, most proteins are not stable under these conditions. This led us to pursue the strategy described in the current work to exploit the very fast kinetics of IEDDAR under physiological conditions. In addition, our strategy differs from those noted above in that it results in minimal background activity in the kidney and hepatobiliary organs as well as other tissues. Drawbacks of our method are the modest radiochemical yields and relatively longer time for synthesis; however, systematic optimization of reaction conditions as well as other parameters should lead to a more efficient and streamlined procedure, which will be explored in future studies.

One of the main motivations for site-specific labeling is that it can provide a more homogeneous product and thereby facilitate clinical translation. In the conjugation of the prosthetic agent to the sdAb, a single product was obtained (Supplemental Fig. 2) whereas products with different levels (and likely sites) of substitution were observed with random lysine modification approaches (*12,14*). The other motivation is to avoid conjugation of the prosthetic agent on a lysine that could alter binding affinity. With 5F7 sdAb, this is a distinct possibility because one of its five lysines is located in CDR2 (*20*). However, a recent study showed no difference in binding affinity for radioiodinated 5F7 conjugates prepared by site-specific and random labeling (*19*), suggesting

either lack of modification or involvement in HER2 recognition for the CDR2 lysine. On the other hand, improvements in binding affinity have been demonstrated for site-specific modification of other sdAbs (*31*), making the affinity advantage possible through this labeling strategy dependent on the characteristics of the particular sdAb.

In previous work, *iso*-[*I]SGMIB emerged as the residualizing agent with the best combination of high tumor retention of radioactivity and low uptake in kidneys (*9*). Accordingly, *iso*-^{125}I-SGMIB-5F7 was selected as the benchmark for use in these paired-label studies evaluating the HER2-targeting potential of ^{18}F-5F7GGC. *In vitro* assays demonstrated HER2-specific uptake of ^{18}F-5F7GGC on HER2-positive BT474M1 cells. Both total cell-associated and internalized activity for ^{18}F-5F7GGC were not significantly different (P>0.05; Fig. 3) from those for co-incubated *iso*-^{125}I-SGMIB-5F7 and increased with time demonstrating that the ^{18}F-prosthetic agent is residualizing. Moreover, with the caveat that assay conditions were not the same, the cellular uptake and internalization of ^{18}F-5F7GGC was similar or higher than that seen previously with 5F7 labeled with ^{18}F using other prosthetic agents (*7,13,14*).

Necropsy and microPET imaging studies demonstrated rapid, high-level accumulation of ^{18}F-5F7GGC in BT474M1 xenografts suggesting that same-day immunoPET imaging would be feasible. This is an important practical advantage compared with intact mAbs like ^{89}Zr-trastuzumab that require up to 6 days to achieve optimal imaging conditions (*32*). Tumor uptake of ^{18}F-5F7GGC was about 20-25% lower than that for co-injected *iso*-^{125}I-SGMIB-5F7, which might reflect the greater residualizing capacity of the guanidino vs. the pyridyl moiety (*33*) and/or the presence of the GK linker (*14*). Nonetheless, with the caveat that different xenograft models were used, ^{18}F-5F7GGC tumor uptake was higher than those reported for most ^{18}F-labeled anti-HER2 sdAb conjugates (*8,12-14,34,35*). A notable exception are the results obtained with ^{18}F-RL-I-5F7 in the same BT474M1 xenograft (*7*); however, even though the less favorable SGMIB isomer (*9*) was used for 5F7 labeling, tumor uptake of radioiodine also was almost two-fold that

observed in the current study for *iso*-^{125}I-SGMIB-5F7. Differences in mouse strain (NOD/SCID versus athymic) between the two studies could play a role (*36*) as could individual xenograft properties like tumor size (*11*), emphasizing the importance of performing experiments in paired-label format when possible.

Importantly, achieving high uptake in tumor with ^{18}F-5F7GGC was not associated with increased uptake in the kidneys or other organs, which might hamper repeated use in patients to monitor HER2 status or interfere with lesion detection. This is an important distinction with agents like ^{18}F-RL-I-5F7, noted above, that show excellent tumor uptake but at the expense of sustained kidney activity levels >100% ID/g (*7*). Indeed, renal activity levels for ^{18}F-5F7GGC were about 4-5 times lower than those for co-administered *iso*-^{125}I-SGMIB-5F7, heretofore possibly the radiolabeled sdAb investigated to date exhibiting the most rapid clearance (*1,9,37*). It is likely that this behavior reflects both the presence of an RBBE-cleavable linker as well as the rapidly clearing 6-^{18}F-fluoronicotinoyl moiety-containing catabolites (*13*). Finally, in our recent study evaluating 5F7 *iso*-^{125}I-SGMIB conjugates formed by different linkers, use of the maleimido linker as done herein resulted in significantly lower kidney uptake compared with the *N*-succinimidyl linker (*19*).

Compounds with both TCO and Tz moieties, especially Tz, are known to accumulate in hepatobiliary organs (*38,39*). For this reason, one of our design considerations was to strategically position the RBBE-cleavable linker in such a way that likely radiolabeled catabolites would be devoid of Tz and TCO moieties. We hypothesized that this would reduce uptake of activity levels in hepatobiliary organs, especially in intestines and gall bladder. Gratifyingly, uptake of activity from ^{18}F-5F7GGC in the gut was more than 5 times lower than observed with a similar construct expected to generate radiolabeled catabolites bearing a Tz moiety (*14*). Consistent with this, while intense gall bladder uptake was observed in the microPET images with the previous ^{18}F-labeled sdAb conjugate (*14*), intestinal and gall bladder uptake was minimal or

not observed for ^{18}F-5F7GGC (Fig. 6). Importantly, the ratios for activity in tumor to liver and to bone, two frequent sites for HER2-positive tumor metastases, were 9:1 and 40:1, respectively, at 1 h after injection.

CONCLUSION

A potentially widely applicable site-specific and residualizing ^{18}F labeling strategy for use with small proteins was validated using anti-HER2 sdAb 5F7. Strategic positioning of an RBBE-cleavable linker provided reduced activity levels in the kidneys and hepatobiliary organs. Moreover, ^{18}F-5F7GGC demonstrated high potential as a probe for immunoPET of HER2-expressing cancers.

DISCLOSURE

This work was supported by NIH Grants CA188177 and CA42324. Michael R. Zalutsky holds ownership interest and is a board member for Cereius, Inc. Ganesan Vaidyanathan is a consultant and shareholder for Cereius, Inc. No other potential conflict of interest relevant to this article was reported.

ACKNOWLEDGEMENTS

The authors thank Dr. Xiao-Guang Zhao, Thomas Hawk and Brian Watts for excellent technical assistance with the animal studies, micro-PET/CT imaging, and SPR, respectively.

KEY POINTS

QUESTION: Can a site-specific linker be devised for ^{18}F-labeling of small proteins that combines tumor-residualizing properties with rapid clearance of activity from kidneys and other normal tissues?

PERTINENT FINDINGS: An anti-HER2 sdAb with a C-terminal cysteine was site-specifically attached with a tetrazine derivative via maleimide-thiol conjugation and labeled with ^{18}F by IEDDAR with a TCO agent attached to an ^{18}F-fluoronicotinoyl moiety via a linker containing a RBBE-cleavable linker. The new ^{18}F-sdAb conjugate exhibited high uptake in HER2-positive tumors with little activity in kidneys and other normal tissues on serial necropsy and microPET imaging.

IMPLICATIONS FOR PATIENT CARE: This site specific and residualizing ^{18}F labeling strategy could facilitate clinical translation of 5F7 anti-HER2 sdAb as well as other sdAbs for immunoPET.

REFERENCES

1. Altunay B, Morgenroth A, Beheshti M, et al. HER2-directed antibodies, affibodies and nanobodies as drug-delivery vehicles in breast cancer with a specific focus on radioimmunotherapy and radioimmunoimaging. *Eur J Nucl Med Mol Imaging.* 2020; Epub ahead of print.

2. Martin V, Cappuzzo F, Mazzucchelli L, Frattini M. HER2 in solid tumors: more than 10 years under the microscope; where are we now? *Future Oncol.* 2014;10:1469-1486.

3. Wolff AC, Hammond MEH, Allison KH, Harvey BE, McShane LM, Dowsett M. HER2 testing in breast cancer: American society of clinical oncology/college of American pathologists clinical practice guideline focused update summary. *J Oncol Pract.* 2018;14:437-441.

4. Xavier C, Vaneycken I, D'Huyvetter M, et al. Synthesis, preclinical validation, dosimetry, and toxicity of ^{68}Ga-NOTA-Anti-HER2 nanobodies for iPET Imaging of HER2 receptor expression in cancer. *J Nucl Med.* 2013;54:776-784.

5. Morris O, Fairclough M, Grigg J, Prenant C, McMahon A. A review of approaches to ^{18}F radiolabelling affinity peptides and proteins. *J Labelled Comp Radiopharm.* 2019;62:4-23.

6. Vaidyanathan G, Zalutsky MR. Synthesis of *N*-succinimidyl 4-[^{18}F]fluorobenzoate, an agent for labeling proteins and peptides with ^{18}F. *Nature Prot.* 2006;1:1655-1661.

7. Vaidyanathan G, McDougald D, Choi J, et al. Preclinical evaluation of ^{18}F-labeled anti-HER2 nanobody conjugates for imaging HER2 receptor expression by immuno-PET. *J Nucl Med.* 2016;57:967-973.

8. Xavier C, Blykers A, Vaneycken I, et al. ^{18}F-nanobody for PET imaging of HER2 overexpressing tumors. *Nucl Med Biol.* 2016;43:247-252.

9. Choi J, Vaidyanathan G, Koumarianou E, Kang CM, Zalutsky MR. Astatine-211 labeled anti-HER2 5F7 single domain antibody fragment conjugates: radiolabeling and preliminary evaluation. *Nucl Med Biol.* 2018;56:10-20.

10. D'Huyvetter M, De Vos J, Xavier C, et al. ^{131}I-labeled anti-HER2 camelid sdAb as a theranostic tool in cancer treatment. *Clin Cancer Res.* 2017;23:6616-6628.

11. Pruszynski M, Koumarianou E, Vaidyanathan G, et al. Improved tumor targeting of anti-HER2 nanobody through *N*-succinimidyl 4-guanidinomethyl-3-iodobenzoate radiolabeling. *J Nucl Med*. 2014;55:650–656.

12. Zhou Z, Devoogdt N, Zalutsky MR, Vaidyanathan G. An efficient method for labeling single domain antibody fragments with ^{18}F using tetrazine-*trans*-cyclooctene ligation and a renal brush border enzyme-cleavable linker. *Bioconjug Chem.* 2018;29:4090-4103.

13. Zhou Z, McDougald D, Devoogdt N, Zalutsky MR, Vaidyanathan G. Labeling single domain antibody fragments with fluorine-18 using 2,3,5,6-tetrafluorophenyl 6-[^{18}F]fluoronicotinate resulting in high tumor-to-kidney ratios. *Mol Pharm.* 2019;16:214-226.

14. Zhou Z, Zalutsky MR, Vaidyanathan G. Labeling a TCO-functionalized single domain antibody fragment with ^{18}F via inverse electron demand Diels-Alder cycloaddition using a fluoronicotinyl moiety-bearing tetrazine derivative. *Bioorg Med Chem.* 2020;28: Epub ahead of print.

15. Chen Z, Chen M, Zhou K, Rao J. Pre-targeted imaging of protease activity through in situ assembly of nanoparticles. *Angew Chem Int Ed Engl.* 2020;59:7864-7870.

16. Gamache RF, Zettlitz KA, Tsai WTK, Collins J, Wu AM, Murphy JM. Tri-functional platform for construction of modular antibody fragments for in vivo ^{18}F-PET or NIRF molecular imaging. *Chem Sci.* 2020;11:1832-1838.

17. Adumeau P, Sharma SK, Brent C, Zeglis BM. Site-specifically labeled immunoconjugates for molecular imaging-Part 1: cysteine residues and glycans. *Mol Imaging Biol.* 2016;18:1-17.

18. Fay R, Holland JP. The impact of emerging bioconjugation chemistries on radiopharmaceuticals. *J Nucl Med.* 2019;60:587-591.

19. Feng Y, Zhou Z, McDouglad D, Meshaw RL, Vaidyanathan G, Zalutsky MR. Site-specific radioiodination of an anti-HER2 single domain antibody fragment with a residualizing prosthetic agent. *Nucl Med Biol.* 2020; Epub ahead of print.

20. Pruszynski M, Koumarianou E, Vaidyanathan G, et al. Targeting breast carcinoma with radioiodinated anti-HER2 nanobody. *Nucl Med Biol.* 2013;40:52-59.

21. Yu Z, Xia W, Wang HY, et al. Antitumor activity of an Ets protein, PEA3, in breast cancer cell lines MDA-MB-311DYT2 and BT474M1. *Mol Carcinog.* 2006;45:667-675.

22. Hamada T, Nishida A, Yonemitsu O. Selective removal of electron-accepting para-toluenesulfonyl and naphthalenesulfonyl protecting groups for amino function via photoinduced donor-acceptor ion-pairs with electron-donating aromatics. *J Am Chem Soc.* 1986;108:140-145.

23. Dornan MH, Simard JM, Leblond A, et al. Simplified and robust one-step radiosynthesis of [^{18}F]DCFPyL via direct radiofluorination and cartridge-based purification. *J Labelled Comp Radiopharm.* 2018:61:757-763.

24. Otaru S, Imlimthan S, Sarparanta M, Helariutta K, Wahala K, Airaksinen AJ. Evaluation of organo [^{18}F]fluorosilicon tetrazine as a prosthetic group for the synthesis of PET radiotracers. *Molecules.* 2020;25:1208.

25. Zettlitz KA, Waldmann CM, Tsai WK, et al. A dual-modality linker enables site-specific conjugation of antibody fragments for ^{18}F-immuno-PET and fluorescence imaging. *J Nucl Med.* 2019;60:1467-1473.

26. Keyaerts M, Xavier C, Heemskerk J, et al. Phase I study of ^{68}Ga-HER2-nanobody for PET/CT assessment of HER2 expression in breast carcinoma. *J Nucl Med.* 2016;57;27-33.

27. Olberg DE, Arukwe JM, Grace D, et al. One step radiosynthesis of 6-[^{18}F]fluoronicotinic acid 2,3,5,6-tetrafluorophenyl ester ([^{18}F]F-Py-TFP): a new prosthetic group for efficient labeling of biomolecules with fluorine-18. *J Med Chem.* 2010;53:1732-1740.

28. Haskali MB, Farnsworth AL, Roselt PD, Hutton CA. 4-Nitrophenyl activated esters are superior synthons for indirect radiofluorination of biomolecules. *RSC Med Chem.* 2020;11:919-922.

29. Glaser M, Iveson P, Hoppmann S, et al. Three methods for ^{18}F labeling of the HER2-binding affibody molecule $Z_{HER2:2891}$ including preclinical assessment. *J Nucl Med.* 2013;54:1981-1988.

30. Iveson PB, Glaser M, Indrevoll B, et al. FASTlab Radiosynthesis of the ^{18}F-labelled HER2-binding affibody molecule [^{18}F]GE-226. *J Labelled Comp Radiopharm.* 2019;62:925-932.

31. Kijanka M, Warnders F-J, El Khattabi M, et al. Rapid optical imaging of human breast tumor xenografts using anti-HER2 VHHs site-directly conjugated to IRDye 800CW for image-guided surgery. *Eur J Nucl Med Mol Imaging*. 2013;40:1718-1729.

32. Ulaner GA, Hyman DM, Ross DS, et al. Detection of HER2-positive metastases in patients with HER2-negative primary breast cancer using ^{89}Zr-trastuzumab PET/CT. *J Nucl Med.* 2016;57:1523-1529.

33. Vaidyanathan G, Affleck DJ, Bigner DD, Zalutsky MR. Improved xenograft targeting of tumor-specific anti-epidermal growth factor receptor variant III antibody labeled using *N*-succinimidyl 4-guanidinomethyl-3-iodobenzoate. *Nucl Med Biol.* 2002;29:1-11.

34. Zhou Z, Chitneni SK, Devoogdt N, Zalutsky MR, Vaidyanathan G. Fluorine-18 labeling of an anti-HER2 VHH using a residualizing prosthetic group via a strain-promoted click reaction: chemistry and preliminary evaluation. *Bioorg Med Chem.* 2018;26:1939-1949.

35. Zhou Z, Vaidyanathan G, McDougald D, et al. Fluorine-18 Labeling of the HER2-targeting single-domain antibody 2Rs15d using a residualizing label and preclinical evaluation. *Mol Imaging Biol.* 2017;19:867-877.

36. Lam K, Chan C, Reilly RM. Development and preclinical studies of ^{64}Cu-NOTA-pertuzumab F(ab')$_2$ for imaging changes in tumor HER2 expression associated with response to trastuzumab by PET/CT. *MAbs.* 2017;9:154-164.

37. Yang EY, Shah K. Nanobodies: next generation of cancer diagnostics and therapeutics. *Front Oncol.* 2020;10:1182.

38. Garcia MF, Gallazzi F, Junqueira MS, et al. Synthesis of hydrophilic HYNIC-[1,2,4,5]tetrazine conjugates and their use in antibody pretargeting with ^{99m}Tc. *Org Biomol Chem.* 2018;16:5275-5285.

39. Ruivo E, Adhikari K, Elvas F, et al. Improved stability of a novel fluorine-18 labeled TCO analogue for pretargeted PET imaging. *Nucl Med Biol.* 2019;76-77:36-42.

FIGURE 1. Scheme for the synthesis of ^{18}F-FN-PEG$_4$-GK-TCO-Tz-PEG$_4$-Mal-5F7GGC (^{18}F-5F7GGC).

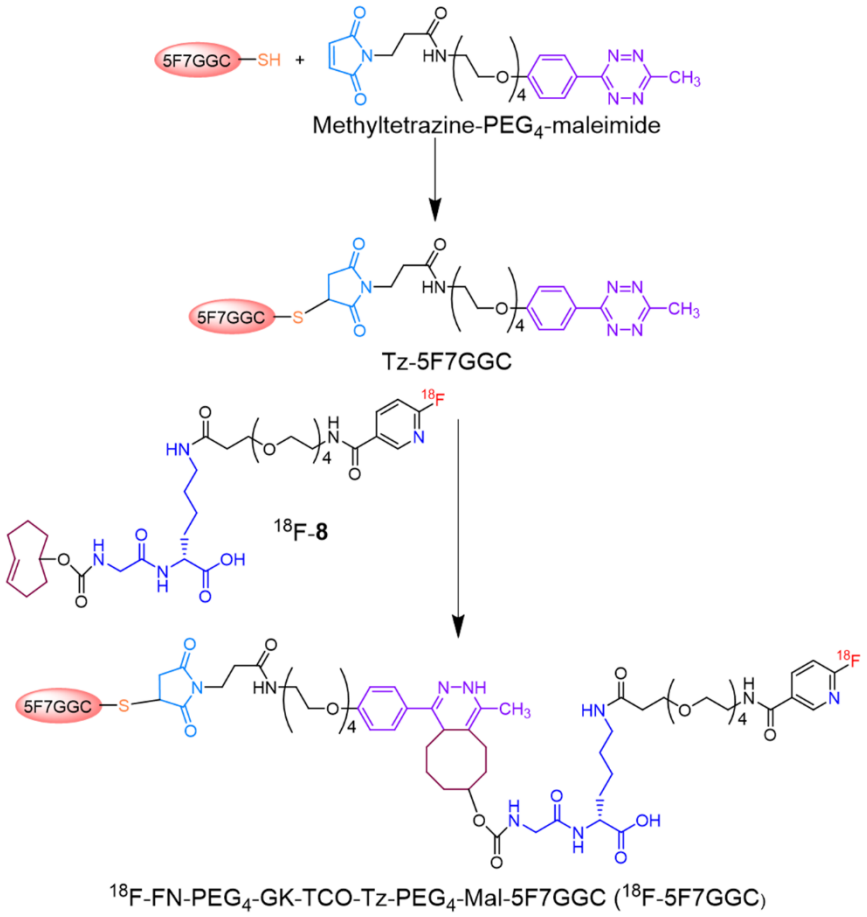

FIGURE 2. Sensorgrams showing dose-response curves and kinetic profiles for the binding of 5F7 (A) and Tz-5F7GGC (B) to HER2-Fc extracellular domain.

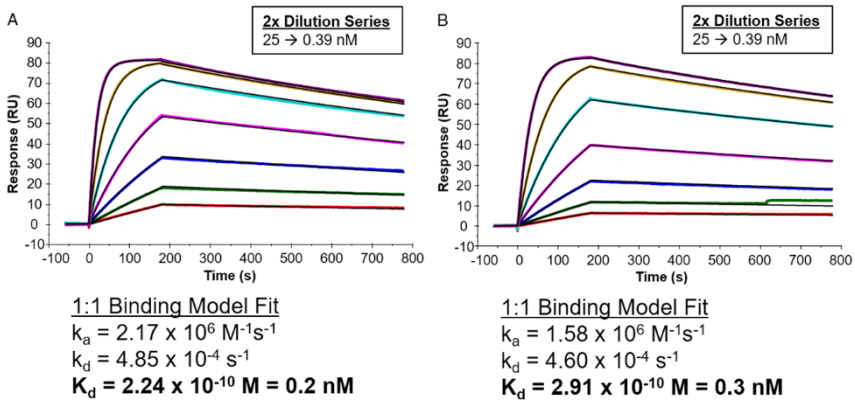

FIGURE 3. Paired-label uptake and internalization of *iso*-^{125}I-SGMIB-5F7 and ^{18}F-5F7GGC by HER2-positive BT474M1 breast carcinoma cells. Data (mean ± SD) are percentage of initially added activity that was (A) bound to cells (membrane + internalized) and (B) internalized.

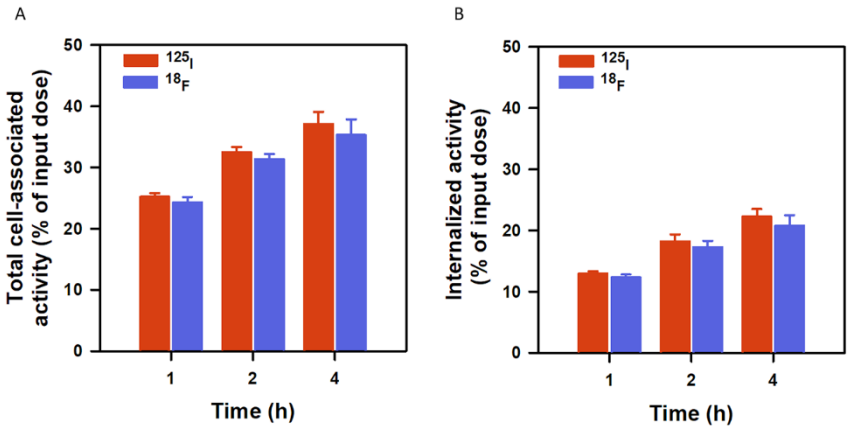

FIGURE 4. Paired-label biodistribution of ^{18}F-5F7GGC and *iso*-^{125}I-SGMIB-5F7 sdAb conjugates in athymic mice bearing subcutaneous HER2-expressing BT474M1 breast carcinoma xenografts.

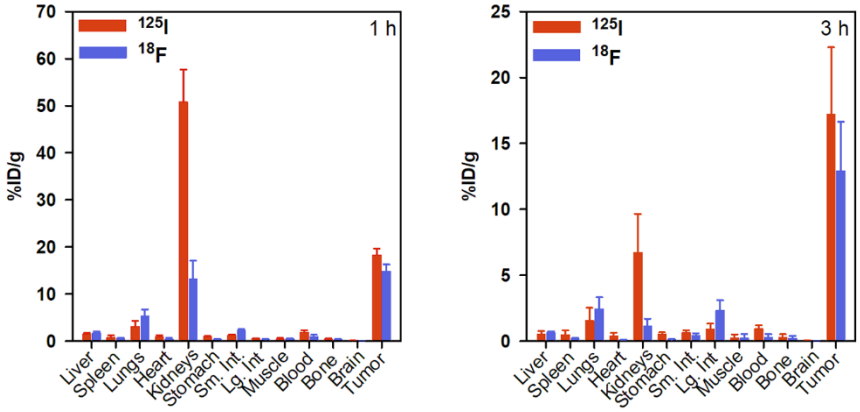

FIGURE 5. Tumor-to-tissue ratios after injection of ^{18}F-5F7GGC and *iso*-^{125}I-SGMIB-5F7 sdAb conjugates in athymic mice bearing subcutaneous BT474M1 xenografts.

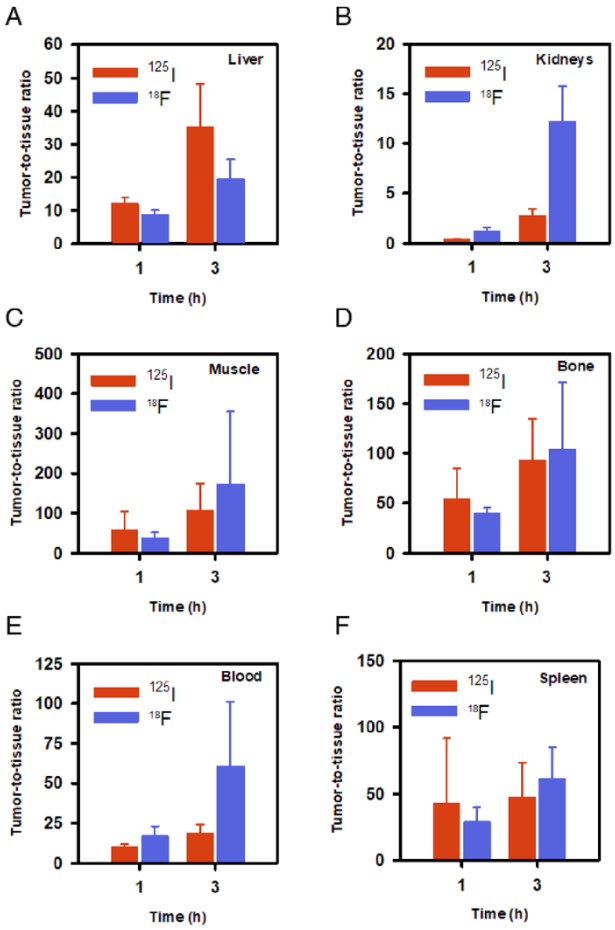

FIGURE 6. Maximum intensity projection ^{18}F-5F7GGC immuno-PET images of a representative mouse bearing subcutaneous HER2-positive BT474M1 xenograft obtained 1, 2, and 3 h post-injection. Positions of tumor (T), kidney (K) and bladder (B) are indicated.

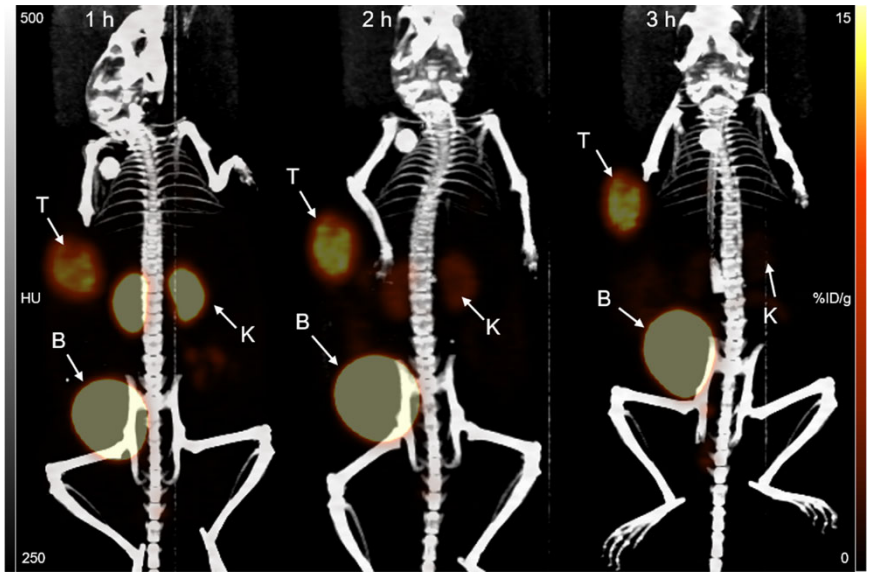

Graphical Abstract

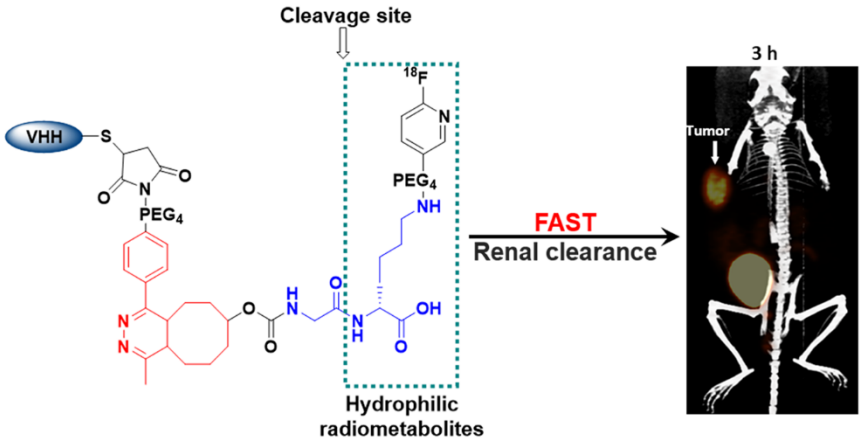

SUPPLEMENTARY MATERIALS

General information

All reagents were purchased from Sigma-Aldrich (St. Louis, MO) except where noted. Sodium ^{125}I-iodide [81.4 TBq (2200 Ci/mmol] in 0.1 N NaOH was obtained from Perkin-Elmer Life and Analytical Sciences (Boston, MA). *N*-succinimidyl 3-((1, 2-bis(*tert*-butoxy-carbonyl)guanidino)methyl)-5-iodobenzoate (Boc_2-*iso*-SGMIB) and its tin precursor *N*-succinimidyl 3-((1, 2-bis(*tert*-butoxycarbonyl)guanidino)methyl)-5-(tri-n-butylstannyl)benzoate (Boc_2-*iso*-SGMTB) were synthesized following reported methods (*1*). N^6-(((9H-fluoren-9-yl)methoxy)carbonyl)-N^2-((*tert*-butoxycarbonyl)glycyl)-L-lysine, **1** (*2*) and *N*,*N*,*N*-trimethyl-5-((2,3,5,6-tetrafluorophenoxy)-carbonyl)pyridin-2-aminium trifluoromethanesulfonate (*3*) were synthesized as previously reported. Methyltetrazine-PEG_4-maleimide and TCO-NHS ester were obtained from Click Chemistry Tools (Scottsdale, AZ), Fmoc-PEG_4-NHS ester from BroadPharm (San Diego, CA) and immobilized tris-[2-carboxyethyl] phosphine hydrochloride gel from Thermo Fisher Scientific (Waltham, MA). HPLC was performed using the following systems: 1) an Agilent 1260 Infinity System (Santa Clara, CA) equipped with a 1260 Infinity Multiple Wavelength Detector, and an Advion Expression^L Compact Mass Spectrometer (Ithaca, NY) in series; 2) an Agilent 1260 Infinity system equipped with a 1260 Infinity multiple wavelength detector and a LabLogic Dual Scan-RAM (Tampa, FL) flow radioactivity detector/TLC scanner. 3) a system similar to that in the second system but with a LabLogic Flow-RAM flow radioactivity detector. The first system was controlled by Advion Mass Express software and the latter two by LabLogic Laura® software. For both radiolabeled and unlabeled compounds, HPLC was performed using an Agilent Poroshell EC-120 (9.4 mm I.D. × 250 mm, 2.7 μm) reversed-phase semi-preparative column. Vivaspin® 500 centrifugal concentrators used for desalting or buffer exchange of the sdAbs were purchased from Sigma-Aldrich (St. Louis, MO). Empore™ SPE C18 cartridges, used for concentrating HPLC samples, were purchased from 3M (Maplewood, MN). Disposable PD-

10 columns for gel filtration were purchased from GE Healthcare (Piscataway, NJ). Activity levels in various samples were assessed using an automated gamma counter — either an LKB 1282 (Wallac, Finland) or a Perkin Elmer Wizard II (Shelton, CT). Proton NMR spectra of samples were obtained on a 400 MHz spectrometer (Varian/Agilent; Inova) and chemical shifts are reported in δ units using the residual solvent peaks as a reference. Mass spectra were recorded using an Advion Expression^{L} Compact Mass Spectrometer for electrospray ionization (ESI) LC/MS (see above) and/or an Agilent LCMS-TOF (ESI); the latter is a high-resolution mass spectrometer. Molecular weights of derivatized sdAbs were determined using the Advion system.

Chemical synthesis

Tert-butoxycarbonyl)glycyl-L-lysine (2)

Compound **1** (300 mg, 0.57 mmol) was dissolved in 2 ml of 20% piperidine in DMF and the mixture stirred at 25°C for 30 min. The solvent was removed under vacuum and the residue was washed with ethyl acetate (3 × 20 ml) to obtain 147.3 mg (0.49 mmol, 85.3%) of compound **2** (*4*) as a white solid: ^{1}H NMR (CD_3OD, 400 MHz) δ_H = 1.3−1.5 (s, 9H), 1.6−1.8 (m, 3H), 2.8−3.0 (t, 3H), 3.6−3.8 (m, 2H), 4.2−4.3 (t, 1H), 8.3−8.4 (s, 1H). LRMS (LCMS-ESI) *m*/*z*: 304.2 $(M+H)^+$. HRMS (ESI, *m*/*z*): calcd for $C_{13}H_{26}N_3O_5$ $(M+H)^+$: 304.1872; found: 304.1861 ± 0.0002 (n = 4).

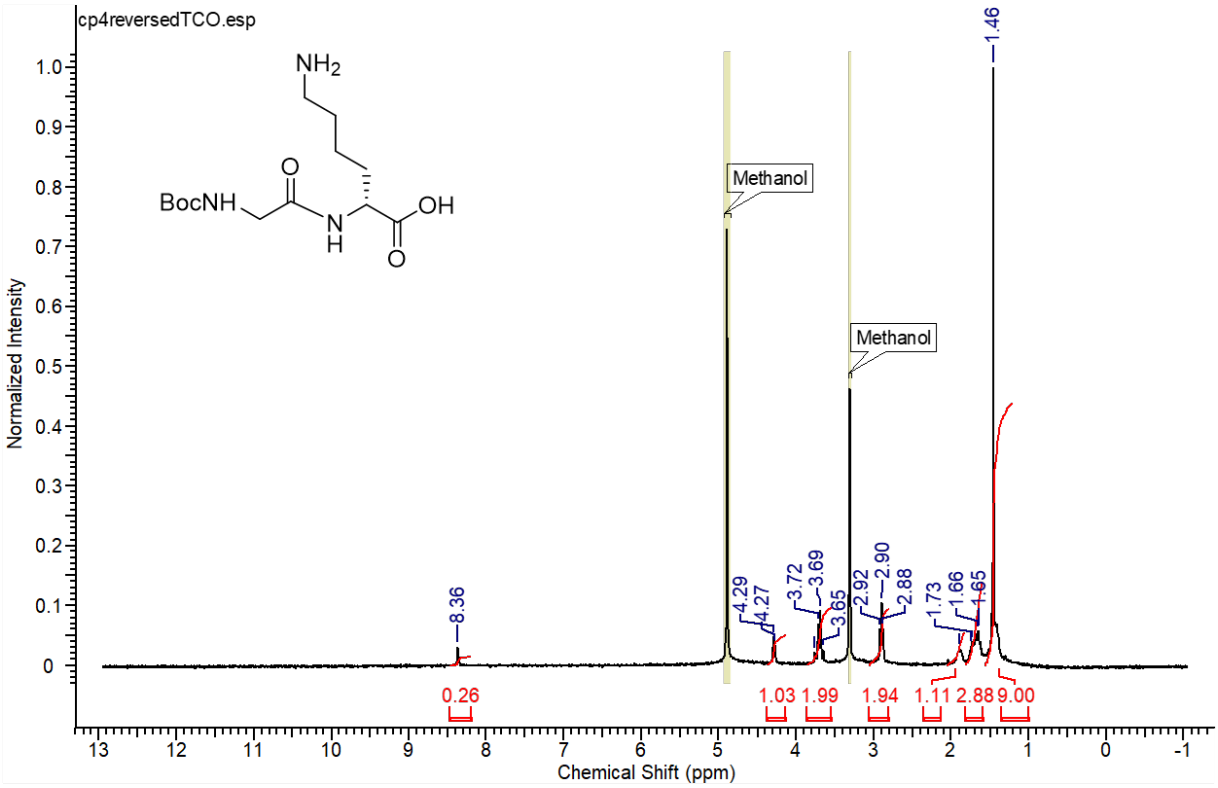

(S)-25-(2-((tert-butoxycarbonyl)amino)acetamido)-1-(9H-fluoren-9-yl)-3,19-dioxo-2,7,10,13,16-pentaoxa-4,20-diazahexacosan-26-oic acid (3)

A mixture of **2** (100 mg, 0.33 mmol), Fmoc-PEG$_4$-NHS ester (193 mg, 0.33 mmol) and *N*,*N*-diisopropylethylamine (41 mg, 0.33 mmol) in 5 ml DMF was stirred at 25°C for 2 h. The crude mixture was purified by semipreparative HPLC. For this, the Agilent Poroshell EC-120 (9.4 × 250 mm, 2.7 µm) reversed-phase semipreparative column was eluted at a flow rate of 4 ml/min with a gradient consisting of 0.1% formic acid both in water (solvent A) and acetonitrile (solvent B); the proportion of B was increased linearly from 30% to 70% over 15 min. Pooled HPLC fractions containing **3** (t_R = 10.0 min) were lyophilized to give 184.2 mg (0.24 mmol, 72.3%) of a white solid: ^{1}H NMR (CD_3OD, 400 MHz) δ_H = 1.3−1.5 (m, 10H), 1.6−1.8 (m, 1H), 1.8−2.0 (m,1H), 2.3−2.5 (t, 2H), 3.1−3.2 (t, 3H), 3.4−3.8 (m, 15H), 4.3−4.5 (m, 3H), 7.2−7.5 (m, 3H), 7.6−7.7 (d, 2H), 7.7−7.9

(d, 2H). LRMS (LCMS-ESI) *m*/*z*: 773.0 $(M+H)^+$. HRMS (ESI, *m*/*z*) calcd for $C_{39}H_{57}N_4O_{12}$ $(M+H)^+$: 773.3973; found: 773.3978± 0.0001 (n = 4).

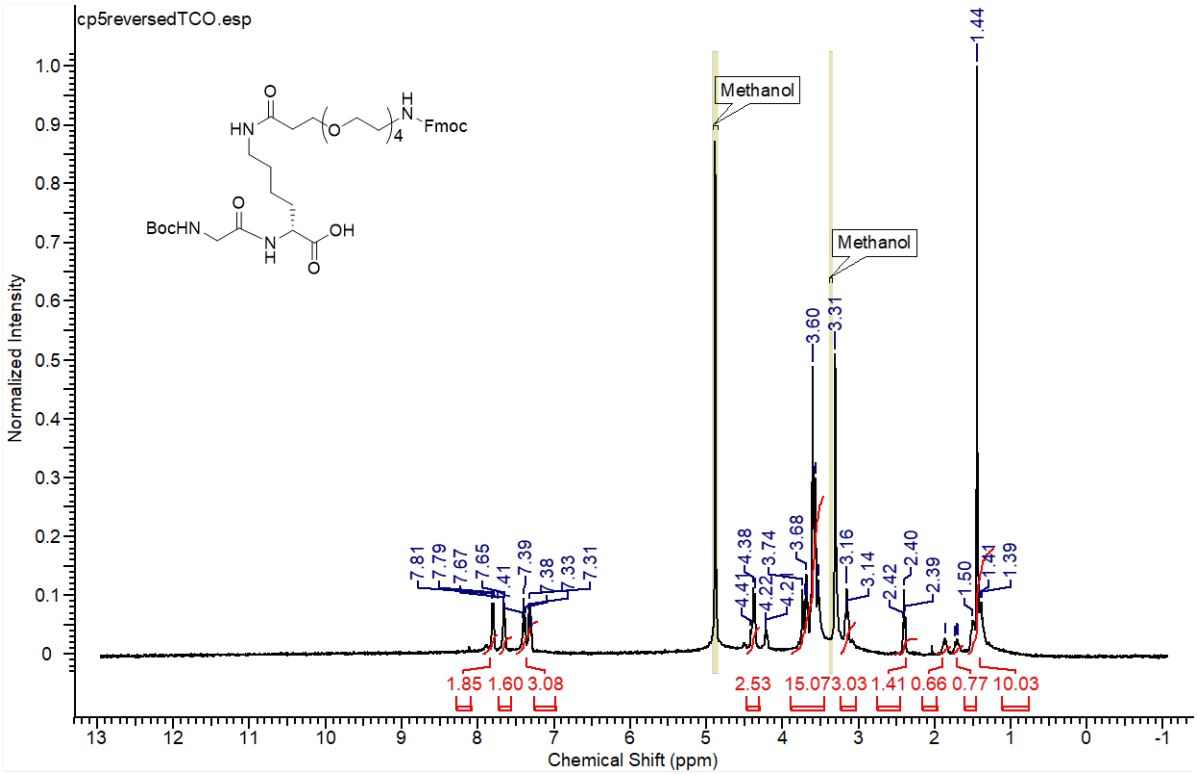

(S)-1-amino-21-(2-((tert-butoxycarbonyl)amino)acetamido)-15-oxo-3,6,9,12-tetraoxa-16-azadocosan-22-oic acid (4)

Compound **3** (100 mg, 0.13 mmol) was dissolved in 2 ml of 20% piperidine in DMF and the mixture stirred at 25°C for 30 min. The solvent was removed under vacuum and the residue washed with ethyl acetate (3 × 20 ml) to obtain 58.3 mg (0.11 mmol, 81.5%) of a colorless oil: ^{1}H NMR (CD_3OD, 400 MHz) δ_H = 1.3−1.6 (m, 13H), 1.6−1.8 (m,1H), 1.8−2.0 (m, 1H), 2.4−2.5 (t, 2H), 3.0−3.2 (m, 6H), 3.6−3.8 (m, 22H), 4.2−4.4 (t, 2H), 8.2−8.3 (s, 2H). LRMS (LCMS-ESI) *m*/*z*: 551.1 $(M+H)^+$. HRMS (ESI, *m*/*z*): calcd for $C_{24}H_{47}N_4O_{10}$ $(M+H)^+$: 551.3292; found: 551.3288 ± 0.0003 (n = 4).

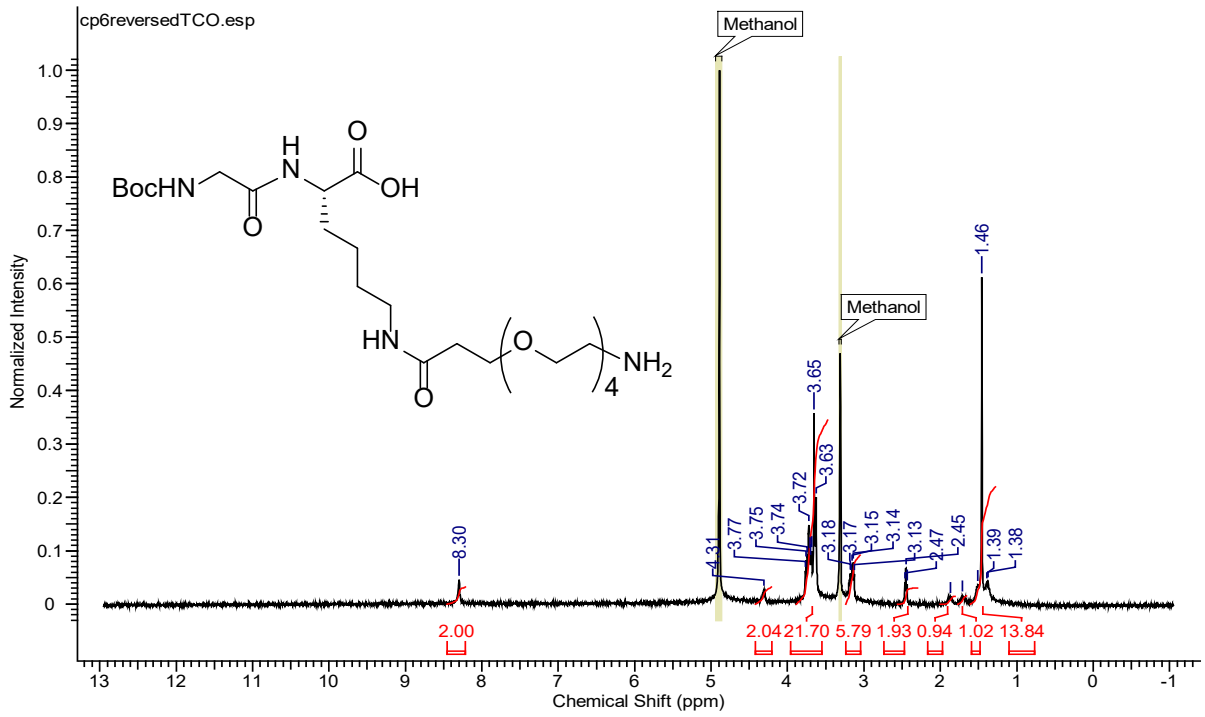

(S)-5-((9-carboxy-2,2-dimethyl-4,7,15-trioxo-3,18,21,24,27-pentaoxa-5,8,14-triazanonacosan-29-yl)carbamoyl)-N,N,N-trimethylpyridin-2-aminium triflate (5)

A mixture of **4** (58.3 mg, 0.11 mmol), *N*,*N*,*N*-trimethyl-5-((2,3,5,6-tetrafluorophenoxy)-carbonyl)pyridin-2-aminium trifluoromethanesulfonate (46.6 mg, 0.10 mmol) and *N*,*N*-diisopropylethylamine (24.8 mg, 0.2 mmol) in 1 ml DMF was stirred at 25°C for 2 h. The product was isolated from this mixture by semi-preparative HPLC as above but using a gradient, wherein the proportion of solvent B was increased linearly from 10% to 30% over 15 min. Lyophilization of pooled HPLC fractions containing **5** (t_R = 12.3 min) delivered 43.5 mg (51.2 µmol, 51.2%) of a white solid: ^{1}H NMR (CD_3OD, 400 MHz) δ_H = 1.2−1.6 (m, 13H), 1.6−1.8 (m, 1H), 1.8−2.0 (m, 1H), 2.3−2.5 (t, 2H), 3.0−3.2 (t, 4H), 3.5−3.8 (m, 30H), 4.2−4.3 (t, 1H), 8.0−8.2 (d, 1H), 8.3-8.4 (s, 1H), 8.5−8.6 (d, 1H), 9.0−9.1 (s, 1H). LRMS (LCMS-ESI) *m*/*z*: 713.5 M^+. HRMS (ESI, *m*/*z*) calcd for $C_{33}H_{57}N_6O_{11}^+$ (M^+): 713.4080; found: 713.4074 ± 0.0001 (n = 4).

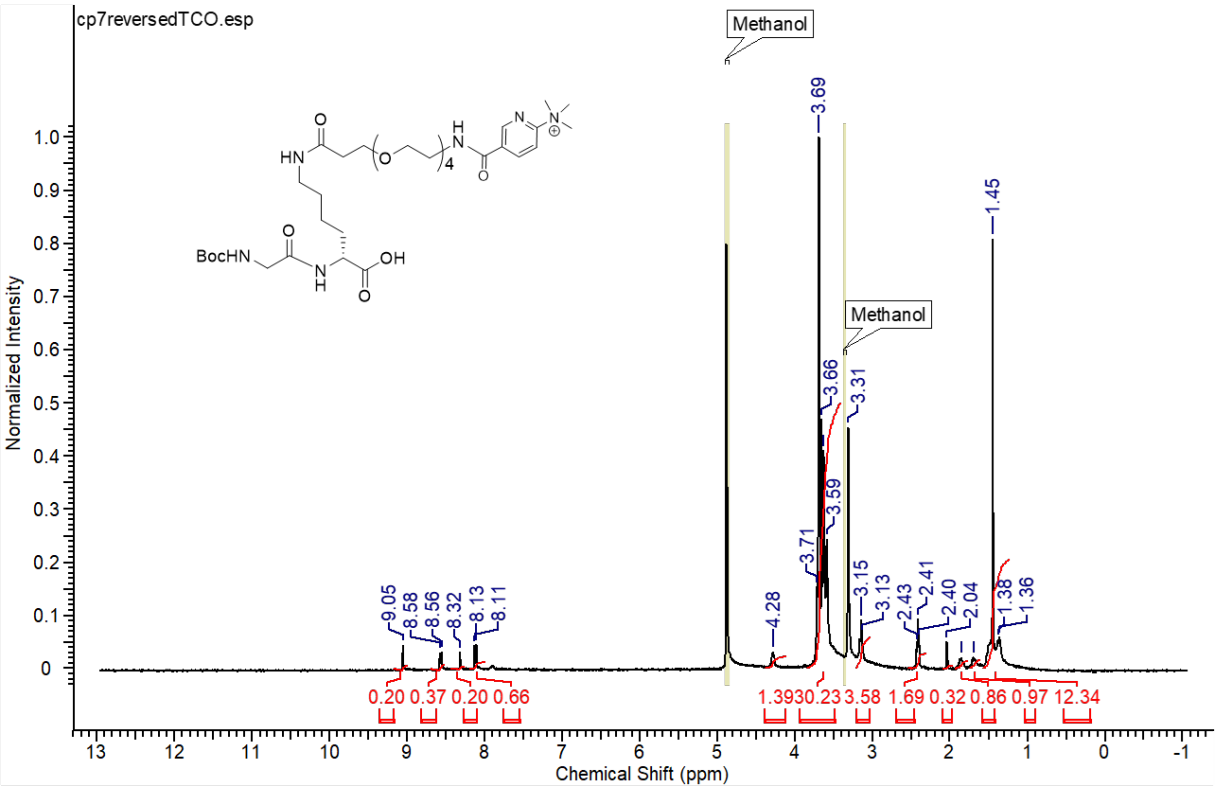

(S)-5-((24-amino-21-carboxy-15,23-dioxo-3,6,9,12-tetraoxa-16,22-diazatetracosyl) carbamoyl)-N,N,N-trimethylpyridin-2-aminium triflate (6)

A 95:2.5:2.5 (v/v/v) mixture of TFA:water:triisopropyl silane (0.5 ml) was added to compound **5** (43.5 mg; 51.2 µmol) and the mixture stirred at 25°C for 30 min. Solvents were evaporated to yield 41.0 mg (92.7%, based on trifluoroacetate salt) of compound **6** as a white solid. Because of its extreme polarity, purification by reversed-phase HPLC was not feasible and thus it was carried over as such to the next step. ^{1}H NMR (D_2O, 400 MHz) δ_H =1.3-1.5 (m, 3H), 2.4-2.5 (t, 1H), 3.1-3.2 (t, 3H), 3.5-3.8 (m, 26H), 3.8-3.9 (s, 2H), 4.3-4.4 (t, 2H), 7.9−8.1 (d, 1H), 8.4-8.5 (d, 1H), 8.9-9.0(s,1H). LRMS (LCMS-ESI) *m*/*z*: 613.5 M^+. HRMS (ESI, *m*/*z*): calcd for $C_{28}H_{49}N_6O_9$ (M^+): 613.3556; found: 613.3552 ± 0.0001 (n = 4).

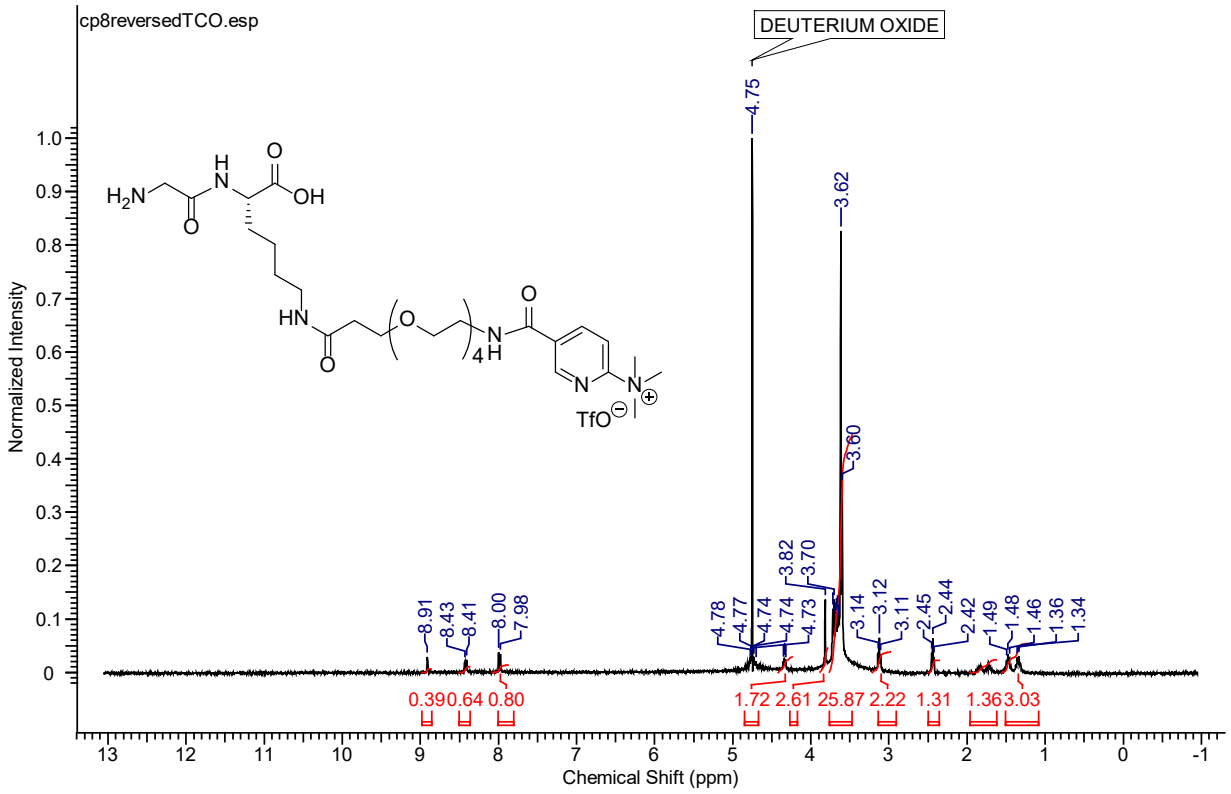

N-(5-(((6S)-6-carboxy-1-(((E)-cyclooct-4-en-1-yl)oxy)-1,4,12-trioxo-15,18,21,24-tetraoxa-2,5,11-triazahexacosan-26-yl)carbamoyl)pyridin-2-yl)-N,N-dimethylmethanideaminium triflate (7)

Compound **6** (41 mg, 53.7 µmol), TCO-NHS ester (19 mg, 71.3 µmol) and *N,N*-diisopropylethylamine (11.8 mg, 95 µmol) were taken in 1 ml DMF and the mixture stirred at 25°C for 2 h. The mixture was subjected to semipreparative HPLC as above but using a gradient wherein the proportion of solvent B was increased linearly from 5% to 30% over 15 min. Lyophilization of pooled HPLC fractions containing **7** (t_R = 14.1 min) rendered 19.5 mg (21.7 µmol, 45.7%) of a colorless oil: ^{1}H NMR (CD_3OD, 400 MHz) δ_H = 1.0−2.0 (m, 14H), 2.25−2.35 (m, 3H), 2.35−2.45 (t, 2H), 3.1−3.2 (t, 4H), 3.5−3.8 (m, 36H), 4.2−4.4 (m, 4H), 5.3−5.7 (m, 4H), 8.0−8.2 (d, 1H), 8.2−8.3 (s, 1H), 8.5−8.6 (d, 1H), 9.0−9.1 (s, 1H). LRMS (LCMS-ESI) *m*/*z*: 765.4 (M^+). HRMS (ESI, *m*/*z*) calcd for $C_{37}H_{61}N_6O_{11}^+$ (M^+): 765.4393; found: 765.4396 ± 0.00004 (n = 4).

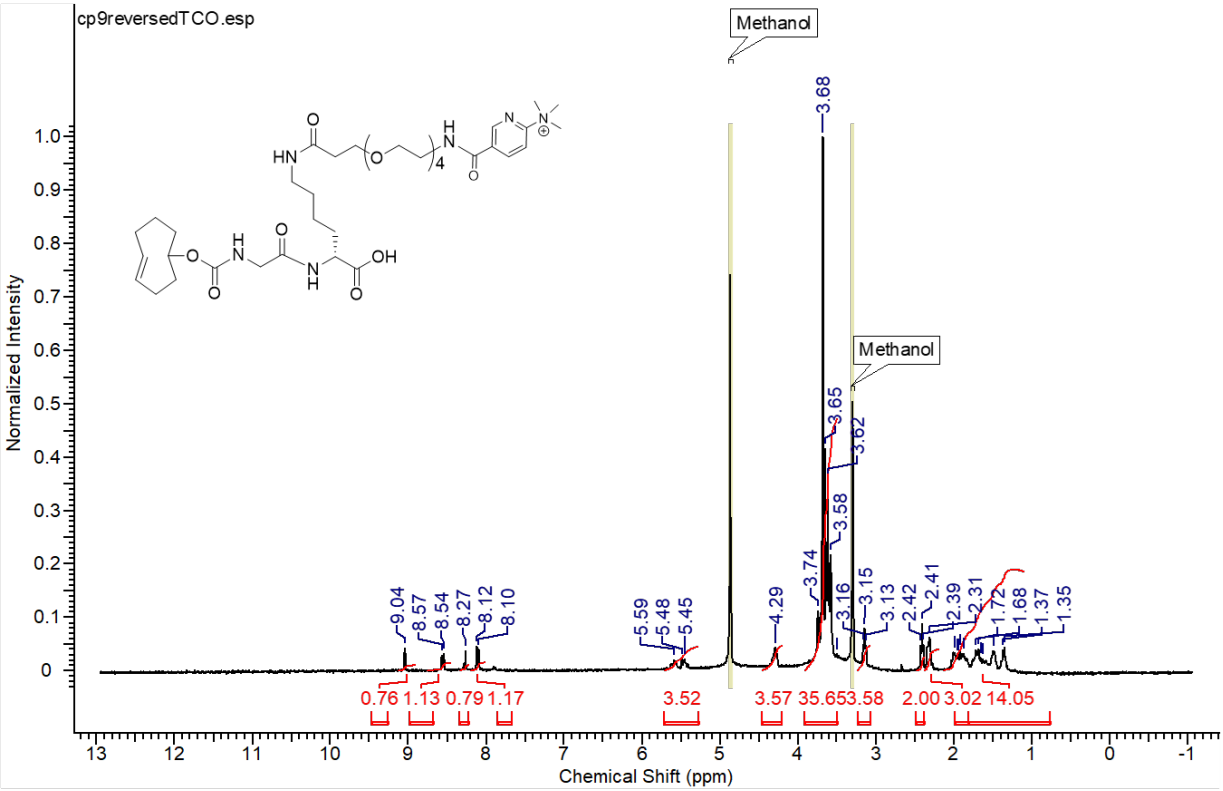

(23S)-23-(2-(((((E)-cyclooct-4-en-1-yl)oxy)carbonyl)amino)acetamido)-1-(6-fluoropyridin-3-yl)-1,17-dioxo-5,8,11,14-tetraoxa-2,18-diazatetracosan-24-oic acid, FN-GK-TCO (8)

A 1M solution (3 µl) of tetra-n-butylammonium fluoride in THF (0.8 mg; 3.0 µmol) was added to a solution of **7** (1 mg, 1.1 µmol) in anhydrous acetonitrile (200 µl), and the mixture stirred at 40°C for 30 min. The resultant product was isolated by semi-preparative HPLC as above but using a gradient wherein the proportion of solvent B was increased linearly from 30% to 70% over 15 min. Solvents from the pooled HPLC fractions (t_R = 9.0 min) were removed by lyophilization to obtain 0.6 mg (0.83 µmol, 75.4%) of **8** as a colorless oil: ^{1}H NMR (CD_3CN, 500 MHz) δH = 1.2-1.8 (m, 13H), 2.2-2.4 (m, 6H), 3.0-3.2 (m, 4H), 3.5-3.8 (m, 21H), 4.1-4.2 (m, 1H), 4.2-4.3(m, 1H), 5.4-5.7 (m, 2), 6.9-7.0 (s, 1H), 7.0-7.1 (m,1H), 7.2-7.4 (s,1H), 8.2-8.5 (m, 2H), 8.7-8.8 (s,1H). LRMS (LCMS-ESI) *m*/*z*: 726.3 $(M+H)^+$. HRMS (ESI, *m*/*z*): calcd for $C_{34}H_{53}FN_5O_{11}$ $(M+H)^+$: 726.3726; found: 726.3725 ± 0.0001 (n = 4).

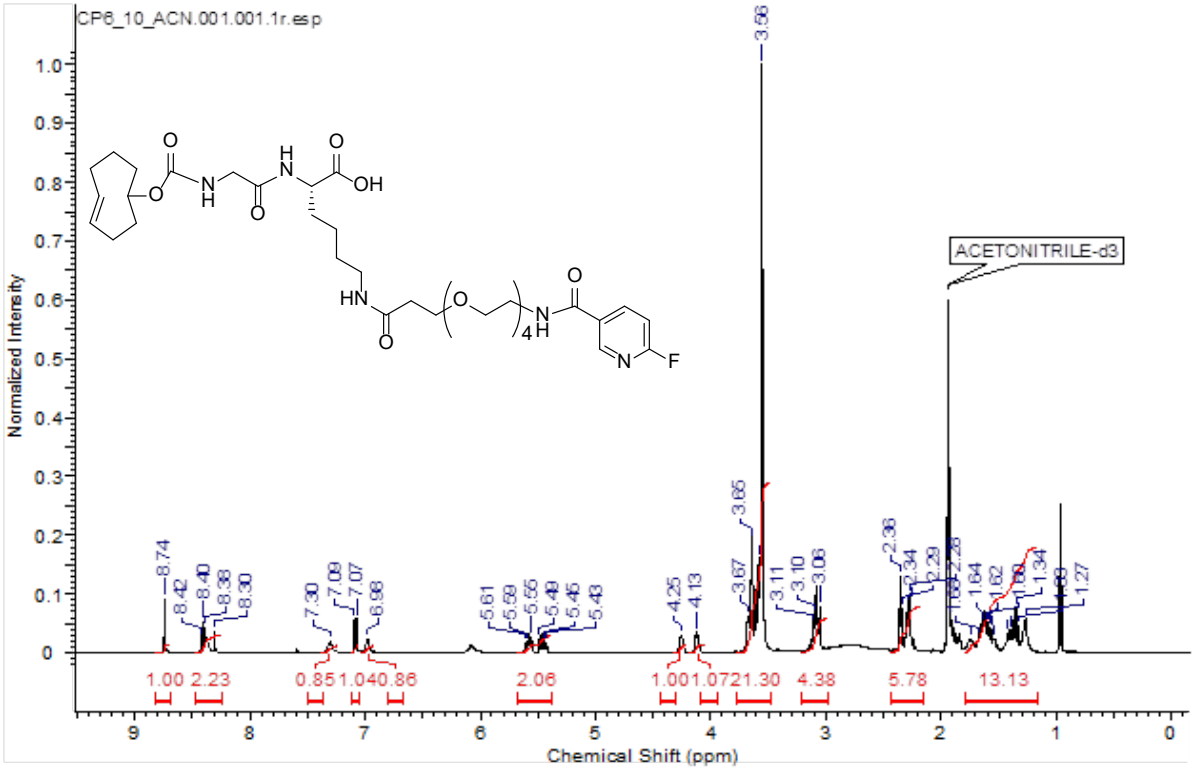

Determination of unlabeled sdAb binding kinetics using surface plasmon resonance

Surface plasmon resonance measurements were performed on a Biacore T200 instrument (Cytiva, Marlborough, MA) at the Duke University Human Vaccine Institute Shared Resource. HER2-Fc protein was immobilized on a CM5 chip via NHS/EDC-mediated amine coupling to 7024 response units (RU). A binding screen of 5F7 and Tz-5F7GGC (50 nM) was performed using the following parameters: 1) flow cells 3 (blank) and 4 (Her2-Fc) (Reference subtraction, 4-3); 2) association and dissociation for each performed for 120 s at 30 µl/min; and 3) regeneration with 10 mM glycine-HCl, pH 2.0 performed for 45 s at 30 µl/min. For the determination of binding kinetics, immobilized Her2-Fc at a lower density (872 RU) was used. Sensorgrams were generated using a 2-fold titration series of each sdAb (0.39–25 nM) with the following parameters: 1) flow cells 1 (blank) and 2 (Her2-Fc) (Reference subtraction, 2-1); 2) 180-s association and 600-s dissociation at 50 µl/min; and 3) regeneration with 10 mM

glycine-HCl, pH 2.0 for 45 s at 30 µl/min. Curves were fit to a 1:1 antigen:analyte binding model using Biacore T200 Evaluation Software to retrieve association rate constants (k_a), dissociation rate constants (k_d), and equilibrium dissociation constants (K_d, a measurement of affinity).

Radiochemistry

Synthesis of ^{18}F-FN-PEG$_4$-GK-TCO (^{18}F-8)

Fluorine-18 activity trapped on a QMA cartridge (Waters Corp, Milford, MA) was obtained from PET-NET Solutions (Durham, NC). The cartridge was eluted with 1 ml of tetraethylammonium bicarbonate in 80% acetonitrile (3 mg/ml). The solvents from the eluate were evaporated at 100°C and the residual water removed by azeotroping with acetonitrile (3 × 0.5 ml) at the same temperature. A solution of **7** (1 mg, 1.1 µmol) in 0.25 ml anhydrous acetonitrile was added to the above dried ^{18}F activity (0.74 – 4.5 GBq), and the mixture heated at 40°C for 15 min. The resultant solution containing ^{18}F-**8** was purified by semi-preparative RP-HPLC as described above for the unlabeled compound using a gradient with the proportion of solvent B increased linearly from 30% to 70% over 15 min. Solvents from the pooled HPLC fractions (t_R = 9.0 min) were concentrated by solid-phase extraction using an Empore™ SPE C18 cartridge eluted with acetonitrile (3 × 150 µl), which was then was evaporated to dryness.

Preparation of iso-^{125}I-SGMIB-5F7

This was performed essentially as described previously (*1,5*). Briefly, Boc$_2$-*iso*-^{125}I-SGMIB (*1,5*) was first deprotected by treatment with TFA and the resultant *iso*-^{125}I-SGMIB was incubated with a solution of 5F7 sdAb in borate buffer, pH 8.5 (2 mg/ml, 50 µl) and the *iso*-^{125}I-SGMIB-5F7 conjugate was isolated by passage through a PD10 column as above.

Evaluation of radiochemical purity, HER2-binding affinity, and immunoreactivity of ^{18}F-5F7GGC

The radiochemical purity of ^{18}F-5F7GGC was determined as described (*2,5*) by SDS-PAGE and size-exclusion HPLC (SE-HPLC). SDS-PAGE was run under non-reducing conditions followed by phosphor imaging using the Storage Phosphor System Cyclone Plus phosphor imager (Perkin-Elmer Life and Analytical Sciences, Downers Grove, IL). SE-HPLC was performed on system 3 using a TSKgel SuperSW2000 (4.6 mm I.D. × 30 cm, 4μm) column (Tosoh Bioscience; Montgomeryville, PA) isocratically eluted with PBS, pH 7.0, at a flow rate of 0.3 ml/min. The binding affinity of ^{18}F-5F7GGC to HER2 on cells was determined by a saturation binding assay using the BT474M line following a reported procedure (*2,5*). Briefly, cells seeded in 24-well plates at a density of 8 × 10^4 cells/well in 0.5 ml of medium were incubated at 37°C overnight. Cells were then incubated at 4°C for 1 h with fresh cold medium containing increasing concentrations (0.1 to 100 nM; 0.6 ml total volume) of ^{18}F-5F7GGC. The cells were washed twice with cold medium, lysed with 0.1% SDS, and the activity in the cell lysates was counted using an automated gamma counter. Non-specific binding was determined in parallel assays performed by co-incubating the cells with a 100-fold excess of unlabeled trastuzumab. The data were fit using GraphPad Prism software to determine K_d values. The immunoreactive fraction of ^{18}F-5F7GGC was determined using magnetic beads coated with HER2 extracellular domain or human serum albumin (HSA) as a negative control as described (*2,5*). The percentage of specific binding (binding to HER2-immobilized minus that to HSA-immobilized beads) was calculated at each bead concentration. The reciprocals of the percentage of specific binding were plotted against the reciprocals of bead concentration, and the data were fit to a straight line by linear regression. The immunoreactive fraction was calculated as the reciprocal of the y-intercept value (infinite antigen concentration).

Paired-label uptake of ^{18}F-5F7GGC and iso-^{125}I-SGMIB-5F7 by BT474M1 cells

HER2-expressing BT474M1 cells (8 × 10^5 cells per well in 2 ml medium) were seeded in 6-well plates and incubated overnight at 37ºC. On the next day, the medium was replaced with 2 ml of medium containing 5 nM each of ^{18}F-5F7GGC and *iso*-^{125}I-SGMIB-5F7, and the cells in

triplicate wells were incubated at 37°C. At 1, 2 and 4 h, the cell culture supernatants were collected, the surface-bound activity was stripped by treating the cells twice with 1 ml of 50 mM glycine, pH 2.8, and finally, the cells were lysed with 0.1% SDS. The activity in the cell culture supernatants, membrane-bound fraction and cell lysates was counted in an automated gamma counter. Cell-associated activity was calculated from these as the percentage of input radioactivity dose associated with the cell lysates. To determine nonspecific uptake, a parallel experiment at the 2-h time point was performed as above but with the addition of a 100-fold molar excess of unlabeled trastuzumab to the incubation medium. The entire experiment was repeated twice.

Supplemental Figure 1. Scheme for the synthesis of quaternary salt precursor, FN-PEG$_4$-GK-TCO, and ^{18}F-PEG$_4$-GK-TCO

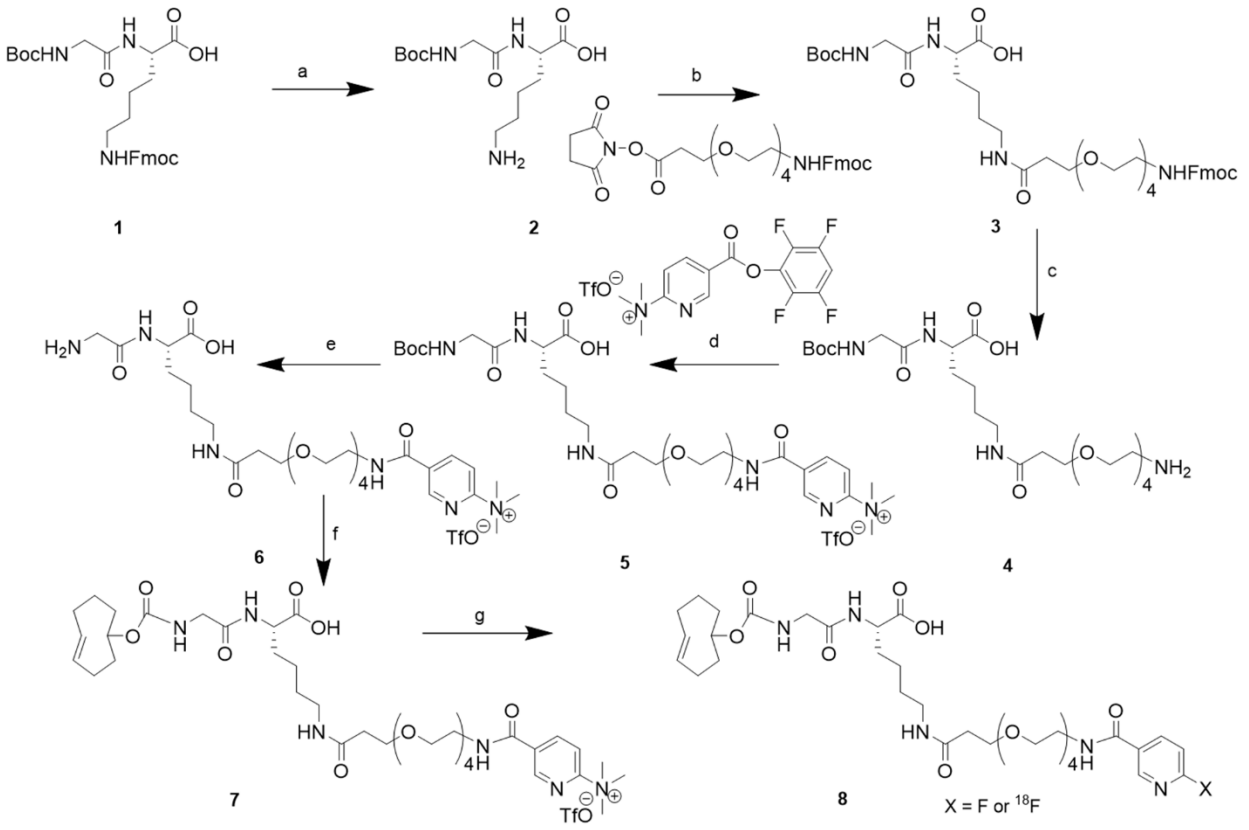

a) 20% piperidine in DMF b) DIEA, DMF c) 20% piperidine in DMF d) DIEA, DMF e) 95:2.5:2.5 TFA:H_2O, Tri-isopropyl silane f) TCO-NHS, DIEA, DMFg) DIEA, DMF h) TBAF or ^{18}F-TEAF, CH_3CN

Supplemental Figure 2: LCMS of Tz- 5F7GGC

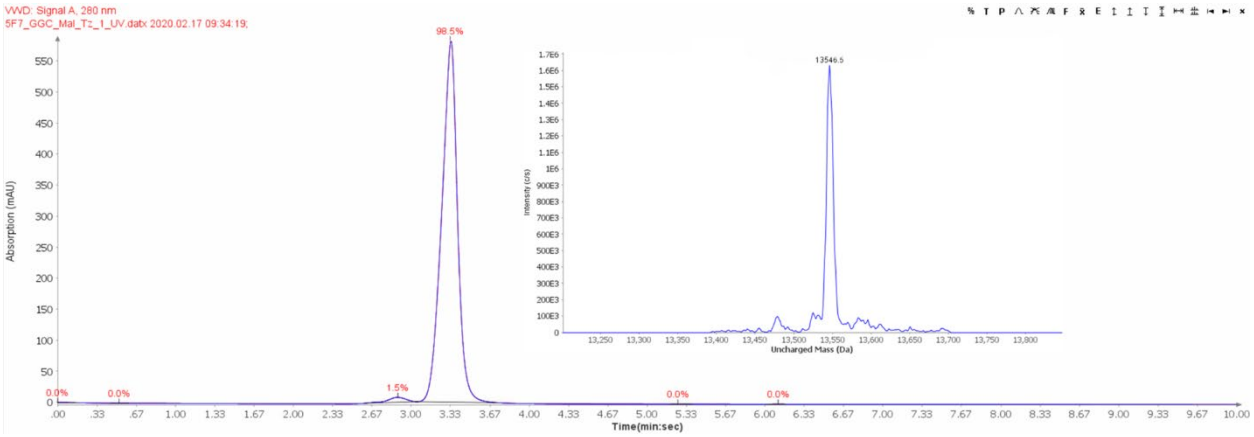

Supplemental Figure 3. Characterization of ^{18}F-5F7GGC conjugate

(A) SDS-PAGE/phosphor imaging of ^{18}F-5F7GGC (right lane) and molecular weight markers (left lane). (B) Size-exclusion HPLC: Radioactivity profile in red and UV profile of molecular weight standards in blue. (C) Saturation binding affinity assay using HER2-positive BT474 cells. (D) Lindmo immunoreactivity assay performed using HER2 ECD- and bovine serum albumin (negative control)-immobilized magnetic beads.

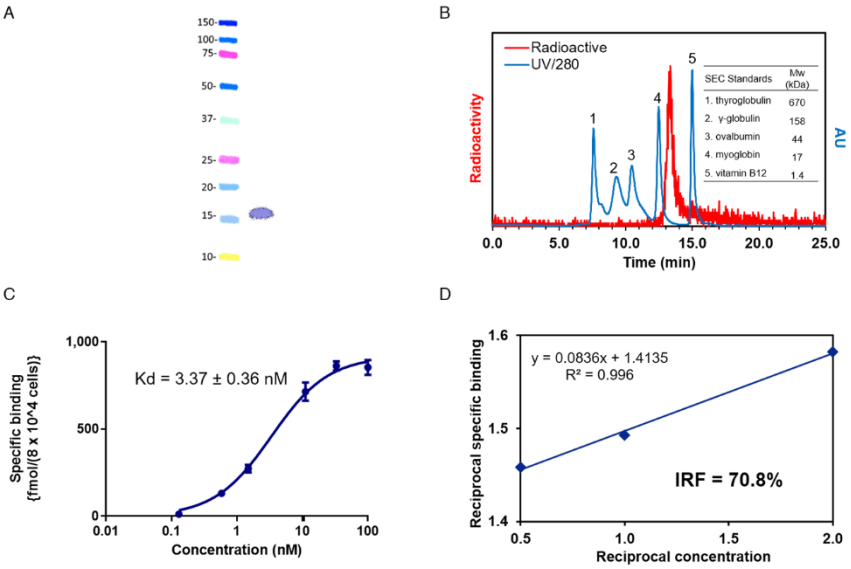

References for supplemental materials

1. Choi J, Vaidyanathan G, Koumarianou E, Kang CM, Zalutsky MR. Astatine-211 labeled anti-HER2 5F7 single domain antibody fragment conjugates: radiolabeling and preliminary evaluation. *Nucl Med Biol.* 2018;56:10-20.

2. Zhou Z, Devoogdt N, Zalutsky MR, Vaidyanathan G. An efficient method for labeling single domain antibody fragments with ^{18}F using tetrazine-*trans*-cyclooctene ligation and a renal brush border enzyme-cleavable linker. *Bioconjug Chem.* 2018;29:4090-4103.

3. Olberg DE, Arukwe JM, Grace D, et al. One step radiosynthesis of 6-[^{18}F]fluoronicotinic acid 2,3,5,6-tetrafluorophenyl ester ([^{18}F]F-Py-TFP): a new prosthetic group for efficient labeling of biomolecules with fluorine-18. *J Med Chem.* 2010;53:1732-1740.

4. Hamada T, Nishida A, Yonemitsu O. Selective removal of electron-accepting para-toluenesulfonyl and naphthalenesulfonyl protecting groups for amino function via photoinduced donor-acceptor ion-pairs with electron-donating aromatics. *J Am Chem Soc.* 1986;108:140-145.

5. Zhou Z, McDougald D, Devoogdt N, Zalutsky MR, Vaidyanathan G. Labeling single domain antibody fragments with fluorine-18 using 2,3,5,6-tetrafluorophenyl 6-[^{18}F]fluoronicotinate resulting in high tumor-to-kidney ratios. *Mol Pharm.* 2019;16:214-226.